

Multi-modal Masked Autoencoders Learn Compositional Histopathological Representations

Wisdom Oluchi Ikezogwo^{*}
 Mehmet Saygin Seyfioglu^{*}
 Linda Shapiro

University of Washington, Seattle, WA 98195, USA

WISDOMIK@CS.WASHINGTON.EDU
 MSAYGIN@CS.WASHINGTON.EDU
 SHAPIRO@CS.WASHINGTON.EDU

Abstract

Self-supervised learning (SSL) enables learning useful inductive biases through utilizing pretext tasks that require no labels. The unlabeled nature of SSL makes it especially important for whole slide histopathological images (WSIs), where patch-level human annotation is difficult. Masked Autoencoders (MAE) is a recent SSL method suitable for digital pathology as it does not require negative sampling and requires little to no data augmentations. However, the domain shift between natural images and digital pathology images requires further research in designing MAE for patch-level WSIs. In this paper, we investigate several design choices for MAE in histopathology. Furthermore, we introduce a multi-modal MAE (MMAE) that leverages the specific compositionality of Hematoxylin & Eosin (H&E) stained WSIs. We performed our experiments on the public patch-level dataset NCT-CRC-HE-100K. The results show that the MMAE architecture outperforms supervised baselines and other state-of-the-art SSL techniques for an eight-class tissue phenotyping task, utilizing only 100 labeled samples for fine-tuning. Our code is available at https://github.com/wisdomikezogwo/MMAE_Pathology

Keywords: histopathology, masked autoencoders, self-supervised learning

1. Introduction

In cancer pathology, tissue phenotyping is essential for learning accurate characterizations of histopathologic biomarkers within the tumor-immune microenvironments. The task of tissue phenotyping with computer vision is a complex endeavor, because the Giga-pixel resolution of whole slide images (WSIs) makes obtaining pixel-level and patch-level annotations challenging. Furthermore, the complexity in morphological phenotypes causes inter and intra-observer variability in tissue labeling.

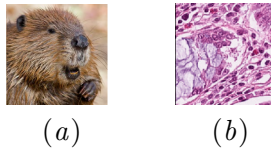


Figure 1: (a): A natural image(b): A histopathology image

Self-supervised learning (SSL) has emerged as an important technique for pre-training

models without the need for large-scale labeled datasets. Instead, the model learns from the unlabeled data by means of a pretext task that utilizes a label generated from the data itself. The SSL framework presents a promising avenue for histopathology since human annotations are extremely costly. Recent SSL research on histopathology focused

^{*} Equal contribution

mostly on contrastive techniques (Yang et al., 2021), (Wang et al., 2021). However, one major drawback of contrastive SSL is that it depends on negative sampling. Negative sampling assumes a relatively good class balance within the dataset such that a sampled mini-batch would consist of images from different classes, which is often not the case for histopathology data. More recently, non-contrastive techniques like DINO (Caron et al., 2021) are adapted to histopathology (Chen and Krishnan, 2022), and require no negative sampling. However, DINO still relies on data augmentation techniques that are specifically designed for ImageNet (coarse-grained object-centric images), and thus is questionable in the context of histopathological images. Also, unlike natural images, WSI patches often have high granularity, as they consist of cells and other cellular structures scattered across a patch Fig 1. Therefore, SSL on WSI patches is a fine-grained embedding learning problem, where data augmentations can be difficult (Xiao et al., 2020).

Recently, a new generative SSL framework Masked Autoencoders (MAE) was introduced (He et al., 2022). MAE forms an encoder-decoder network (both of which are a Vision Transformer (ViT), (Dosovitskiy et al., 2020), then masks random patches of a given input image and reconstructs the masked patches using the visible ones. MAE needs no negative samples and does not depend on extensive data augmentations, thus it is very suitable for histopathology data. However, similar to the case of contrastive learning (Stacke et al., 2021), heuristics in MAE designed for natural images do not necessarily transfer to histopathology, so more research is needed for adapting MAE to histopathology applications. By keeping the encoder fixed, we experimented with three different design choices for MAE: masking ratio, decoder depth, and patch size. For the

patch size, what is the optimal ViT patch size for WSIs? Should it be sub-cell size or larger? For the masking ratio, there is a trade-off: Since patch-level WSIs have high granularity, too much masking would make it impossible to extrapolate, and too little masking would result in trivial interpolation. So what is the optimal masking ratio? Moreover, does a deeper decoder help in downstream phenotype classification task? To find the optimal design choices we designed a set of experiments and proposed a multi-modal MAE (MMAE) that implicitly leverages human domain knowledge by incorporating H-stain, and E-stain images in addition to RGB, which helps the model to further leverage cross-modal interactions for better feature learning.

Our contributions are two-fold. First, we perform experiments to answer the above questions in the design of the MAE architectures for tissue phenotyping using patch-level WSIs. Second, we propose the MMAE architecture that exploits human domain knowledge through the use of H&E stain inputs, which provides compositional histomorphological information in regards to cell and stroma. We compare our results against DINO, CS-CO and from-scratch supervised approaches on a patch-level phenotyping task using a public dataset CT-CRC-HE-100K. Our results show that MAE outperforms contrastive/non-contrastive energy-based SSL techniques. Furthermore, we show that MAE’s performance can be improved through the use of domain knowledge in the MMAE setting, which relies on a masking strategy that condenses all patch positions and samples uniquely from each modality. This allows for lighter masking ratios, which capture the granular nature of patch-level WSIs across all modalities.

2. Related Work

Many SSL approaches have been developed for natural images. Earlier works like inpainting (Pathak et al., 2016), colorization tasks (Zhang et al., 2017), Jigsaw puzzle solving (Noroozi and Favaro, 2016) and rotation prediction (Gidaris et al., 2018) learned good features for semantic understanding. However, contrastive methods such as SimCLR (Yang et al., 2021), based on minimizing the distance between augmented views of the same image and maximizing the distance between different images within a mini-batch, mostly dominated the field. Recently, DINO (Caron et al., 2021) a non-contrastive method, which uses student-teacher distillation to learn part-whole relationships between the augmented views, was introduced.

SSL methods have also been applied to the histopathology domain, mostly with contrastive learning. In the CS-CO method, (Yang et al., 2021) proposed a contrastive SSL model with a novel augmentation method called stain vector perturbation. (Gildenblat and Klaiman, 2019) implemented a contrastive loss based on the spatial distance of patches, i.e. closer patches are considered as positives and farther ones as negatives. Although these methods are somewhat shown to improve performance in detecting morphological phenotypes, they relied on DA methods that were specifically designed for object-centric coarse-grained natural images, thus the assumptions behind these DA techniques do not always transfer well to pathology (Stacke et al., 2021). Contrastive SSL generally learns inductive biases through the use of DA techniques, which implicitly injects human domain knowledge. However, it is generally hard to engineer augmentation techniques in histopathology as the downstream tasks show great dissimilarity. For example, in the case of scoring of immunohistochemical staining, color

might be an important feature, so augmenting with color jittering would improve the downstream performance. However, in the case of tumor classification, color jittering may downgrade the performance and thus should not be shared among positives. Finding good hard negatives also remains very challenging, especially in histopathology where patch-level WSIs are much more homogeneous compared to natural images. Lastly, negative sampling assumes a good class balance within the dataset. However, it is hard to argue that this will be valid for patch-level WSIs where there is an imbalance between morphological phenotypes (Chuang et al., 2020). Recently, non-contrastive techniques, such as DINO, are also adapted on histopathology data (Chen and Krishnan, 2022). However, DINO still relies on extensive DA techniques, and also requires a lot of hyperparameters to be tuned, which makes it cumbersome to train. Therefore, a framework that does not rely on extensive augmentation techniques and negative sampling would be a better fit for histopathology data, and MAE perfectly fits this role.

3. Methodology

In section 3.1 we focus on the MAE architecture. Next, in section 3.2 we introduce the multi-modal MAE, which leverages multi-modal inputs for the reconstruction task.

3.1. Masked Autoencoders

Masked Autoencoders (MAE) is a generative SSL technique that yields state of the art performance in ImageNet benchmarks (He et al., 2022). MAE randomly masks a portion of the patches of the input image, feeds the unmasked (visible) patches to its ViT encoder, and then reconstructs the masked patches using a lightweight ViT decoder by optimizing a mean squared error loss \mathcal{L}_{MSE} . Unlike contrastive models, it does not require neg-

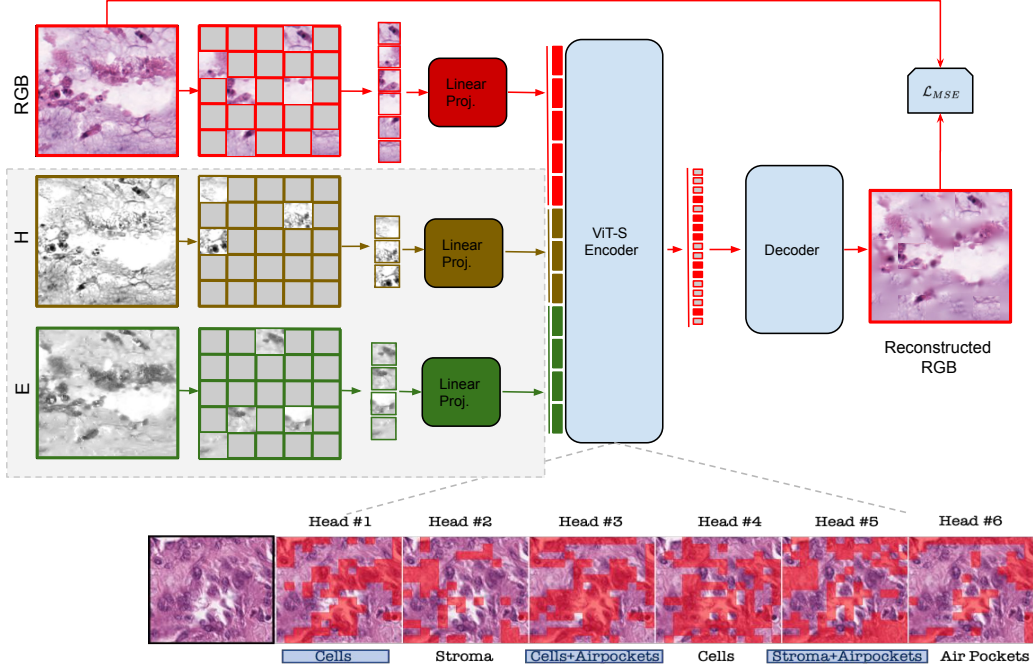


Figure 2: MMAE architecture During pre-training, similar to Large language models, and unlike natural image vision models, a small random subset of patches (e.g. 25%) is masked out. **Interpretation** Thresholded visualization of multi-head attention weights shows that MMAE learns to localize different histo-morphological features like cells in #1, 3 and 4, stroma tissue in #2 and 3, and regions of fat/air-pockets in #3, 5 and 6, provides empirical evidence that MMAE can capture important inductive biases about histopathology tissue compositionality.

ative sampling, requires little to no augmentations, and has a few hyperparameters to be tuned. Overall, it has three components: the patchifying layer, the encoder, and the decoder.

Masking. As in the case of ViT, an input image is patchified by using convolutions with a kernel size of $(\mathcal{P}, \mathcal{P})$ and stride of \mathcal{S} into \mathcal{N} non-overlapping patches. Then randomly selected patches are sampled without replacement and masked. The number of patches to be masked is fixed such that the encoder always receives the same amount of patches in every iteration.

Encoder. MAE’s backbone encoder is a ViT, which takes non-masked input patches. Each visible patch is first flattened into a vector embedding by a linear projection, then a

2D sinusoidal position embedding is added to it. The resulting vectors are then processed by the Transformer blocks.

Decoder. Similar to the encoder, the decoder also consists of Transformer blocks, with the task of reconstructing the masked patches using the latent variables created by the encoder. At the final layer, the decoder uses a linear projection to reconstruct the pixel values for each masked patch. The decoder is only used during pre-training and removed in the downstream fine-tuning.

3.2. Multi-Modal MAE

Inspired by (Bachmann et al., 2022), we propose a Multi-Modal MAE (MMAE) that leverages H&E stains in addition to RGB inputs. The overall architecture of our MMAE

differs from (Bachmann et al., 2022) as we do not do multi-task reconstruction (no reconstruction for H&E inputs), so we have a single decoder that is dedicated to RGB reconstruction. We argue that, by incorporating H&E stains, we are infusing the domain knowledge, since H&E stains highlight different histomorphological features (e.g cell and stroma morphology). Thus using the tokens (patches) from H&E allows us to further reduce masking of RGB tokens, since it is nontrivial to reconstruct the RGB tokens using H&E tokens. The overall architecture is shown in Fig 2.

MMAE Masking. Similar to (Bachmann et al., 2022), we use a Dirichlet distribution to determine the amount of visible tokens for each modality by sampling from $Dir(\alpha)$ distribution, which is controlled by the concentration parameter $\alpha > 0$, where larger α means more tokens will be sampled from that modality, and equal α 's between modalities mean a uniform sampling. To be specific, we sample points from a Dirichlet distribution and multiply those floats by our total number of tokens to get the number of samples per task to use as input. A difference in our sampling strategy from that of (Bachmann et al., 2022) is that they sample randomly across their input modalities, which generally results in the same patch position being taken in more than one modality. However, since WSIs are highly granular, we need visible tokens to be complementary, thus information coming from additional modalities must be ensured. To provide that, we implemented the *mask-one* strategy, which ensures that unique tokens will be selected across all modalities. (For details about the *mask-one* strategy, see Appendix.)

MMAE Encoder. MMAE utilizes separate linear projections for each input, then adds position embeddings on top of each patch vector, and concatenates the resulting vectors. Concatenated patch vectors are

then fed into the same Transformer architecture used as given in the MAE encoder. No modality specifying token is used explicitly, however the concatenation is always sequenced in the same fashion: first the unmasked tokens from RGB and then H and E are combined together.

MMAE Decoder. Our MMAE decoder aims to reconstruct only the RGB input, so unlike (Bachmann et al., 2022), we use one decoder. We add a single cross-attention layer in the decoder to stimulate cross-modal interaction between the latent variables from each input modality.

4. Experiments

We designed a set of experiments by utilizing a ViT-S backbone with 12 layers and 6 attention heads (each with dimension of 64) as our encoder. For MAE, we experimented with three different hyperparameters: patch size, decoder depth, and masking ratio, while keeping the two fixed and varying the remaining one. For MMAE, we kept the best hyperparameters that we gathered from the MAE experiments for decoder depth and patch size, and experimented with different masking and sampling strategies on the MMAE where we tried a) equal masking for all modalities, b) heavy masking on RGB and light masking on H&E, and c) heavy masking on H&E and light masking on RGB.

Dataset. We trained and validated our models on the NCK-CRC-100K dataset of 100,000 histological images of human colorectal cancer and healthy tissue, extracted as 224×224 patches at 0.5 microns per pixel (MPP) with 8 classes. The final sizes of the training and test sets are 89,434 and 6333, respectively, and the evaluation measure is the eight-class classification accuracy of the test set; see Appendix for details.

H&E Stain Separation. Different dyes are employed in histology to emphasize vari-

ous types of tissue components, which might be considered domain-specific knowledge implicit in histopathological images (Alturkistani et al., 2016). In our case, cell nuclei will be stained purple by hematoxylin, while the extracellular matrix and cytoplasm will be stained pink by eosin in the commonly used H&E stain. Hematoxylin and eosin stain results are referred to as H channel and E channel stain image, respectively. Similar to the work by (Yang et al., 2021) we use the Vahadane approach (Vahadane et al., 2016) for stain separation to restore single-dye staining results from H&E stain images and to reduce stain variance. Vahadane casts the stain separation problem as a sparse non-negative matrix factorization (SNMF) with L1 sparse regularization. See Appendix for a detailed mathematical explanation.

Pre-training and Downstream Fine-tuning Details. We pre-train the models for 1600 epochs using four NVIDIA A4000 GPUs with automatic mixed precision enabled. With a base learning rate (lr) of $1e-4$ and weight decay of 0.05, we employ the AdamW optimizer. We warm up training for 40 epochs, starting with a lr of $1e-6$ and decaying it to 0 using cosine decay during the length of training. For the augmentations, we randomly crop the patches with a random scale between 0.8 and 1.0, crop to 224×224 pixels and apply a random horizontal flip with a probability of 0.5. (See Appendix for the full list of hyperparameters). For the downstream, we fine-tune for the 8-class classification by replacing the decoder with an average pooling operation, averaging over all encoded tokens, followed by Layer-Norm and a linear projection. The encoder is fine-tuned for 100 epochs, using 5-fold cross validation in all settings. Also, rather than using the entire training set, we randomly select 100 and 1000 samples from the training set, and fine-tune with this group to better represent each method’s representation ca-

pacity. Also, note that for the MMAE fine-tuning, we only utilize the RGB inputs. We compare our results against DINO, a non-contrastive energy-based model, and CS-CO, a contrastive model. For DINO, we use the settings given in (Chen and Krishnan, 2022), and for CS-CO, we report results directly from (Yang et al., 2021).

5. Results

5.1. MAE Results

Decoder Depth. For decoder depth experiments, we kept the masking ratio at 75% and patch size at 16×16 . We fine-tuned the pre-trained MAE model using $N = 100$, and $N = 1000$ samples in two different experiments. The results are shown in Fig 4.

Patch Size. We experimented with the patch sizes of 8×8 , 14×14 , and 16×16 by keeping the decoder depth at 2, and masking ratio at 75% and results are shown in Fig 5.

Masking Ratio. Perhaps the most important hyperparameter in the MAE setting is the masking ratio. We experimented with a large set of masking ratios, keeping the patch size at 16×16 and decoder depth at 2. Results show that histopathology data shows different behavior compared to natural images as expected, where higher masking ratios result in sub-optimal performance, especially when fine-tuned with a small amount of samples. Results are shown in Fig 6.

5.2. MMAE Results

Masking Ratio and Masking Strategies. First, we experimented with different masking strategies on different modalities based on $Dir(\alpha)$. Results show that heavy masking on E&H, and light masking on RGB works better than other strategies. Specifically, we found that $\alpha_{RGB} = 0.8$, $\alpha_H = 0.1$, and $\alpha_E = 0.1$ is the optimal setting.

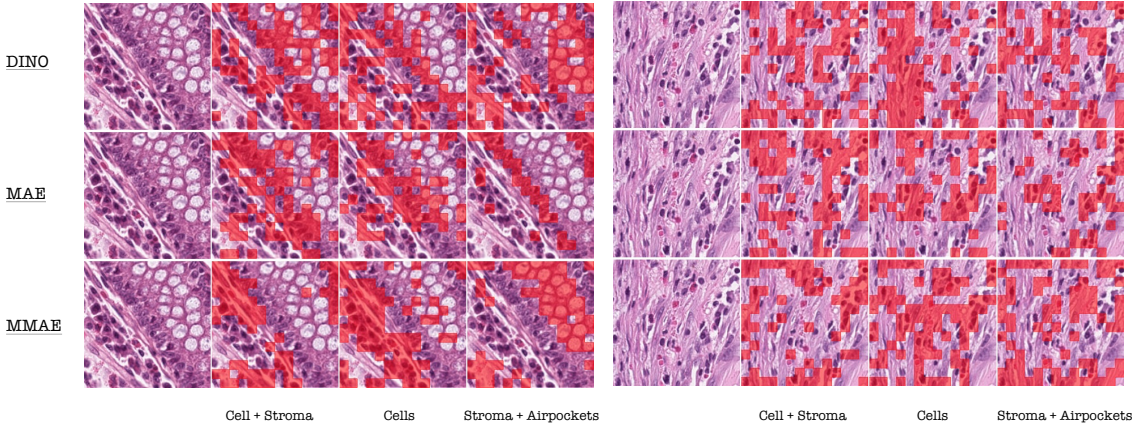


Figure 3: **Attention Visualizations** for MMAE, MAE, and DINO. We extract visualizations from the final attention layer’s first, third, and fifth heads. We see MMAE focuses on varying morphological features in each head more clearly than MAE or DINO.

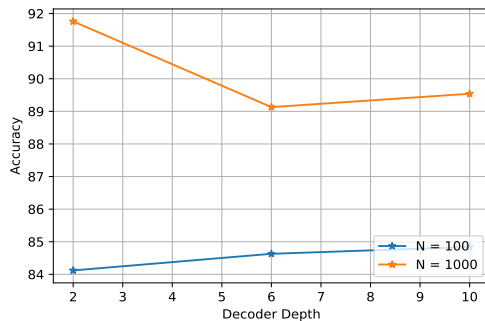


Figure 4: Results for Decoder Depth

Then we experimented with different masking ratios using the optimal masking strategy. We found that the MMAE allows us to reduce the masking ratio further, as it yields its best performance using 190 tokens (which are 80% from RGB and 20% from E&H, on average). The results for masking ratios on MMAE is shown on Fig 7.

5.3. Results Compared Against Other SSL Methods

Our results in Table 1 indicate that both MAE and MMAE outperform other SSL

methods and from-scratch baselines for the eight-class tissue phenotyping task. We also see that MMAE slightly outperforms MAE, as it allows us to reduce the overall masking ratio to better capture the granular nature of patch-level WSIs, while increasing the individual masking applied to RGB, thereby alleviating the risk of trivial interpolation.

Table 1: Accuracy results obtained with 5-fold cross-validation; note that from-scratch accuracy is 85.52% using the whole dataset.

Models	$n = 100$	$n = 1000$
DINO	89.65	92.61
CS-CO	83.40	91.51
MAE	91.98	93.01
MMAE	92.29	93.34

Pre-training Performance Comparison Against DINO. We set up additional experiments to evaluate the pre-training performance of MMAE by nearest neighbor matching against DINO, the runner-up of our benchmarks. MMAE outperforms DINO in the nearest neighbor matching setting, where DINO yields around 87% for 10 nearest neighbors (NN) and 87.45% for 20 NNs,

whereas MMAE yields 90.19% and 90.94%, for NN=10 and NN=20, respectively.

To visually evaluate the models, we visualized the attention distributions across attention heads of the encoders of the MAE, MMAE and DINO models, which is shown Fig 3 (See Appendix for more attention visualizations). Furthermore, we used UMAP to visualize the representation quality of the embeddings, which can be seen in Fig 8.

6. Discussion

6.1. MAE Hyperparameters

Masking Ratio. Our results indicate that heavy masking performs poorly for patch-level WSIs as opposed to natural images. For coarse-grained natural images, it is easy for the model to extrapolate using fewer patches, since a single object can be inferred utilizing a limited signal. However, patch-level WSIs have a higher degree of granularity, where different cellular structures are scattered across the patches. Thus, the model requires more visible patches for learning the cellular structures. Also, masking too lightly yields poor results, as having too many visible adjacent patches leads to trivial interpolation, which aligns with the findings in natural images (He et al., 2022). Interestingly,

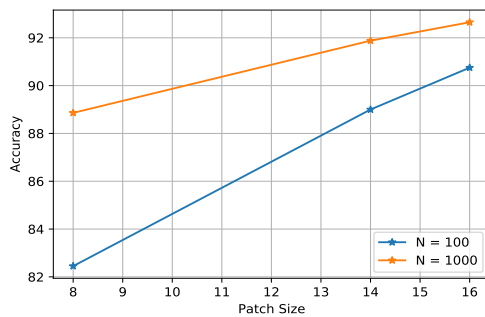


Figure 5: Results for Patch Sizes

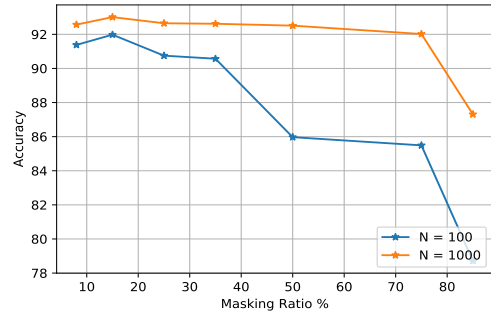


Figure 6: Results for Masking Ratios for MAE

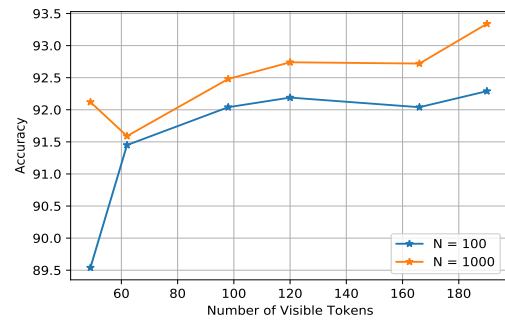


Figure 7: (Number of Visible Tokens used in MMAE (Note that 80% of the visible tokens are from RGB)

optimal masking ratios for patch-level WSIs are similar to masked language modeling in natural language processing, where the typical masking ratio is also around 15%.

Decoder Depth. We found that increasing the depth of the decoder brings mixed results. Though it provides a slight performance boost when fine-tuned with N=100 samples, it degrades performance when fine-tuned with N=1000 samples, and it is computationally expensive. So, similar to the case of natural images, the decoder of MAE should also be shallow when trained with patch-level WSIs. We argue that, given the capacity, the decoder may be leaning towards

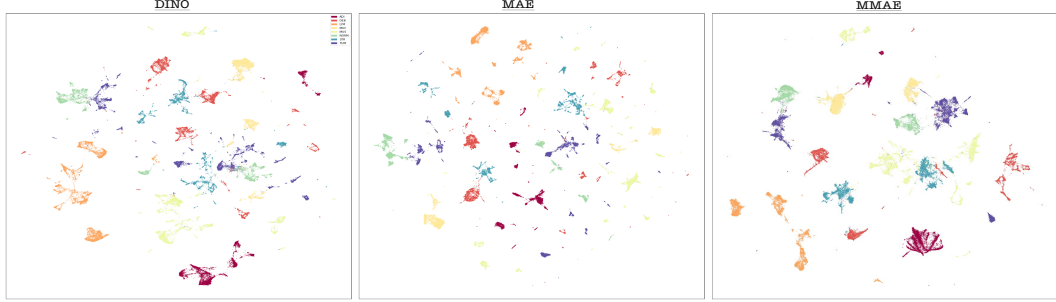


Figure 8: Using the default UMAP parameters ($neighbors = 15, dist = 0.1$) we obtained the 2D scatter plots for DINO, MAE, and MMAE using the [CLS] tokens of each model. For all 8-classes **A**, MMAE clusters them into separable groups, which implies MMAE learns better representations for tissue phenotypes in comparison to DINO.

learning shortcut features that render the feature learning on the encoder somewhat less critical.

Patch Size. We found that the optimal patch size for WSIs is 16×16 , the same as for natural images. We argue that if cell-sized or sub cell-sized patches are employed, as in the case of the 8×8 patches, the reconstruction task becomes a trivial interpolation. Then, even higher masking ratios do not help, because sub-patch level information makes it too easy to learn any useful inductive biases.

6.2. Multi-modal MAE

Masking Strategies and Masking Ratios. Results indicate that light masking on RGB and heavy masking on E&H (providing more visible tokens from RGB and less from E&H) outperforms equal masking in all modalities, as well as the heavy masking on RGB and light masking on E&H cases. We argue that since the pre-training task is to reconstruct the RGB input, the model requires more tokens to have a general understanding of it. Moreover, since our fine-tuning objective utilizes only RGB inputs, the model needs to have more familiarity with them.

Also, the results show that MMAE outperforms other SSL methods. We observe that MMAE relaxes the masking trade-off, as it allows us to use more visible tokens overall than MAE. However, note that MMAE uses less visible RGB tokens, so the extra tokens come from E&H. This helps the model better capture the granular nature of the WSIs without risking trivial interpolation. Since E&H images encode different information and are disparate from the RGB image, reconstructing RGB tokens using E&H is not straightforward. By using fewer RGB tokens than MAE (without the expense of signal loss), MMAE better captures the cell structure, and thus outperforms in both fine-tuning and nearest neighbor matching tasks.

6.3. Limitations and Conclusions

There are some limitations of this work. First, we did not perform a comprehensive hyperparameter search to determine the combinations of design choices for MAE, as pre-training requires too much compute time. Second, NCK-CRC-100K is a relatively small dataset, so the experiments must be re-conducted on a larger dataset to vali-

date the effectiveness of MAE and MMAE in the histopathological setting.

In closing, our work shows the effectiveness of generative pre-training with MAE compared to other SSL techniques. We highlight that MAE benefits from low masking ratios for patch-level WSIs. Lastly, we show that the performance of MAE can be further improved by incorporating H&E stains in the MMAE setting, which provide compositional signals that hold cellular information and allow us to further reduce the masking ratio to better capture the granular nature of patch-level WSIs.

References

Hani A Alturkistani, Faris M Tashkandi, and Zuhair M Mohammedsaleh. Histological stains: a literature review and case study. *Global journal of health science*, 8(3):72, 2016.

Roman Bachmann, David Mizrahi, Andrei Atanov, and Amir Zamir. Multimae: Multi-modal multi-task masked autoencoders. *arXiv preprint arXiv:2204.01678*, 2022.

Mathilde Caron, Hugo Touvron, Ishan Misra, Hervé Jégou, Julien Mairal, Piotr Bojanowski, and Armand Joulin. Emerging properties in self-supervised vision transformers. In *Proceedings of the IEEE/CVF International Conference on Computer Vision*, pages 9650–9660, 2021.

Richard J Chen and Rahul G Krishnan. Self-supervised vision transformers learn visual concepts in histopathology. *arXiv preprint arXiv:2203.00585*, 2022.

Ching-Yao Chuang, Joshua Robinson, Yen-Chen Lin, Antonio Torralba, and Stefanie Jegelka. Debiased contrastive learning. *Advances in neural information processing systems*, 33:8765–8775, 2020.

Alexey Dosovitskiy, Lucas Beyer, Alexander Kolesnikov, Dirk Weissenborn, Xiaohua Zhai, Thomas Unterthiner, Mostafa Dehghani, Matthias Minderer, Georg Heigold, Sylvain Gelly, et al. An image is worth 16x16 words: Transformers for image recognition at scale. *arXiv preprint arXiv:2010.11929*, 2020.

Spyros Gidaris, Praveer Singh, and Nikos Komodakis. Unsupervised representation learning by predicting image rotations. *arXiv preprint arXiv:1803.07728*, 2018.

Jacob Gildenblat and Eldad Klaiman. Self-supervised similarity learning for digital pathology. *arXiv preprint arXiv:1905.08139*, 2019.

Kaiming He, Xinlei Chen, Saining Xie, Yanghao Li, Piotr Dollár, and Ross Girshick. Masked autoencoders are scalable vision learners. In *Proceedings of the IEEE/CVF Conference on Computer Vision and Pattern Recognition*, pages 16000–16009, 2022.

Mehdi Noroozi and Paolo Favaro. Unsupervised learning of visual representations by solving jigsaw puzzles. In *European conference on computer vision*, pages 69–84. Springer, 2016.

Deepak Pathak, Philipp Krahenbuhl, Jeff Donahue, Trevor Darrell, and Alexei A Efros. Context encoders: Feature learning by inpainting. In *Proceedings of the IEEE conference on computer vision and pattern recognition*, pages 2536–2544, 2016.

Karin Stacke, Jonas Unger, Claes Lundström, and Gabriel Eilertsen. Learning representations with contrastive self-supervised learning for histopathology applications. *arXiv preprint arXiv:2112.05760*, 2021.

Abhishek Vahadane, Tingying Peng, Amit Sethi, Shadi Albarqouni, Lichao Wang, Maximilian Bautz, Katja Steiger, Anna Melissa Schlitter, Irene Esposito, and Nassir Navab. Structure-preserving color normalization and sparse stain separation for histological images. *IEEE transactions on medical imaging*, 35(8):1962–1971, 2016.

Xiyue Wang, Sen Yang, Jun Zhang, Minghui Wang, Jing Zhang, Junzhou Huang, Wei Yang, and Xiao Han. Transpath: Transformer-based self-supervised learning for histopathological image classification. In *International Conference on Medical Image Computing and Computer-Assisted Intervention*, pages 186–195. Springer, 2021.

Tete Xiao, Xiaolong Wang, Alexei A Efros, and Trevor Darrell. What should not be contrastive in contrastive learning. *arXiv preprint arXiv:2008.05659*, 2020.

Pengshuai Yang, Zhiwei Hong, Xiaoxu Yin, Chengzhan Zhu, and Rui Jiang. Self-supervised visual representation learning for histopathological images. In *International Conference on Medical Image Computing and Computer-Assisted Intervention*, pages 47–57. Springer, 2021.

Richard Zhang, Phillip Isola, and Alexei A Efros. Split-brain autoencoders: Unsupervised learning by cross-channel prediction. In *Proceedings of the IEEE conference on computer vision and pattern recognition*, pages 1058–1067, 2017.

Appendix A.

Dataset Details NCK-CRC-100K is annotated with the following non-overlapping tissue classes: adipose (Adi), background (Back), debris (Deb), lymphocytes (Lym), mucus (Muc), smooth muscle (Mus), normal colon mucosa (Norm), cancer-associated stroma (Str), colorectal adenocarcinoma epithelium (Tum). We experiment on CRC-100K without Macenko SN. When evaluating visual representation learning methods, we don’t use images from the background (BACK) class for training and testing. This is because they are always non-informative, and can be easily predicted using simple threshold based approaches (Yang et al., 2021; Chen and Krishnan, 2022).

Stain separation formulation Elaborating mathematically, let $I \in \mathbb{R}^{m \times n}$ be the RGB intensity matrix, $V \in \mathbb{R}^{m \times n}$ be the relative optical density, $W \in \mathbb{R}^{m \times r}$ be the stain color matrix, and $H \in \mathbb{R}^{r \times n}$ be the stain concentration matrix for an H&E stained image, where $m = 3$ for RGB images, r is the number of stains, and n is the number of pixels. The relationship between V and H, W can be stated as $V = \log \frac{I_0}{I} = WH$, where $I_0 = 255$ for 8-bit RGB pictures, according to the Beer-Lambert law. Then, W and H can be estimated by solving the sparse non-negative matrix factorization problem as Eq. (1) proposed by (Vahadane et al., 2016).

$$\begin{aligned} \min_{W, H} \frac{1}{2} \|V - WH\|_F^2 + \lambda \sum_{j=1}^r \|H(j, :)\|_1 \\ \exists W, H \geq 0, \quad \|W(:, j)\|_2^2 = 1 \end{aligned} \quad (1)$$

The H channel and E channel images I_h and I_e can be recovered as $I_h = I_0 \exp(-H[0, :])$ and $I_e = I_0 \exp(-H[1, :])$, respectively, using the estimated stain concentration matrix H . See Fig 2 for RGB, H and E images.

Sampling Strategy Depicted in Fig 9-a, *Mask-all* effectively treats each patch position in all three modalities equally, thus making the sampling space equal to the total number of patches available ($3 * M$). Using our best MAE mask ratio of 15% would mean encoding ≈ 500 patches, which would lead to inefficiencies due to the quadratic memory and compute constraints of self-attention. However, with *Mask-one*, due to the compositional nature of H and E images, we can reduce our sampling space to M by sampling each unique patch position just once 9.

Algorithm 1: Mask-One sampling strategy

```

Algorithm maskOne()
1 | task.tokens ← List[Dir(o) tokens per task]
2 | patch_ids ← {Set of all unique patch positions}
3 | task_ids = []
4 | N ← length(task.tokens)
5 | for modal ← 0 to N do
   | | task_ids ← append(sample_wo_replacement(patch_ids, task.tokens/modal))
| end
| return task_ids
Procedure sample_wo_replacement(sample_list, num)
1 | sample ← num elems sampled randomly from sample_list w/o replacement
   | (inplace).
2 | return sample

```

Training details In Table 2 we report the changes to the default pre-training setting in (Bachmann et al., 2022).

Hyperparameters	Value
Pre-training	
Base lr	1e-4
Batch size	312
Augmentation	RandomResizedCrop (scale: 0.8, 1.0)
Num. global tokens	1
Epochs	1600
Sampling α	$\alpha_{RGB}: 8, \alpha_H : 1, \alpha_E : 1$
Norm pix loss	True
Patch size	8, 14, 16
Decoder depth	2, 6, 10
Fine-tuning	
Base lr	3e-3
Weight decay	6e-5
Batch size	96
Epochs	100

Table 2: Pre-training settings.

Figure 9: (a) MMAE sampling strategies: In this simple (4x4) grid setting, the grids show selected patch positions for each modality (b) We provide more attention visualizations for all 8-classes.

